04

Determination of optimal spatial orientation of photorefractive crystal GaAs at contradirectional four-wave mixing

© V.N. Naunyka

Mozyr State Pedagogical University named after I.P.Shamyakin,
Mozyr, Republic of Belarus

e-mail: valnav@inbox.ru

Received January 05, 2025
Revised February 21, 2025
Accepted February 21, 2025

The dependence of the reflection coefficient at contradirectional four-wave mixing in the photorefractive semiconductor GaAs on its spatial orientation is theoretically investigated. The coupled waves equations were used for the calculations, in the derivation of which it was assumed that secondary mixed holographic gratings with a phase-amplitude structure are formed in the crystal. The theoretical model took into account the combined contribution of the linear electro-optical, photoelastic, and inverse piezoelectric effects, as well as the natural absorption of the recording medium. It was found that when using the GaAs semiconductor, the maximum diffraction efficiency at contradirectional four-wave mixing is achieved in the case when the normal to the cut plane of the crystal is oriented along one of the ⟨234⟩ directions. In the case when the normal to the cut plane is directed along ⟨112⟩ and ⟨111⟩, the reflection coefficient can reach 90% and 80% of the maximum possible value, respectively.

Keywords: Four-wave mixing, phase-conjugation front, photorefractive crystal, reflection coefficient, coupled wave equations.

DOI: 10.61011/EOS.2025.11.62921.7524-25

Introduction

Photorefractive crystals (PRCs) are widely used as photosensitive recording elements in the creation of holographic interferometers, optical radiation filters, holographic memory systems, and optical modulators [1]. Studies of the propagation and interaction features of photorefractive optical spatial solitons have demonstrated the promise of using PRCs in the development of modern optical networks and waveguides [2]. Recent publications [3–5] have shown the principal feasibility of using PRCs in the development of artificial intelligence and machine learning systems. The authors of [3] presented a prototype of a photonic photorefractive switching matrix designed for training neural networks. The normal operation of the photorefractive components of the matrix and the successful transmission of signals through the optical processor were experimentally confirmed. In [4,5], it was shown that soliton-based photorefractive neural networks, which mimic the functional behavior of biological neural tissue, can potentially be used for bit-by-bit information storage and recognition. The neural network changes and adapts to input signals, storing and recognizing them through photorefractive nonlinearity, which is functionally analogous to biological neuroplasticity. Contemporary advances in studying the diffraction and interaction patterns of light waves on dynamic photorefractive gratings, as well as the technological capabilities of using PRCs in optical applications, can be found in [6,7].

The discovery of wavefront reversal in four-wave mixing (FWM) in a dynamic medium, described in the pioneering work [8], led to the development of new methods for controlling the spatial structure of light beams, optical processing, and information recording (see, e.g., [9]). The use of PRCs as a dynamic recording medium for wavefront reversal stimulated the creation of lasers with dynamic gratings, which allow fine tuning of the emission frequency during generation [10]. At present, several research groups continue to investigate the patterns of FWM on dynamic photorefractive gratings. The features of theoretical modeling of energy exchange between light waves in degenerate FWM in a photorefractive recording medium were studied in [11]. The authors examined the limits of applicability of the undepleted pump approximation in analyzing wavefront reversal features in PRCs using the method of small perturbations. In [12] the authors studied the possibility of suppressing turbulence in coherent free-space optical channels using the phase conjugation effect in degenerate FWM. The ability to automatically suppress turbulence in a coherent line was demonstrated through the implementation of self-pumped phase conjugation in a PRC. The authors of [13] investigated methods for slowing optical pulses via nonlinear dispersion in nondegenerate frequency FWM in the semiconductor CdTe. It was shown that the holographic setup configuration can be adjusted such that the phase-conjugate wave arising in FWM is slowed, while the transmitted wave is accelerated.

The semiconductor GaAs is one of the widely used photorefractive materials in optical applications due to its high holographic recording speed and holographic sensitivity close to the theoretical limit [14]. The appeal of this PRC

stems from the possibility of shifting into the infrared spectral range when used as a nonlinear recording medium. The study [15] is devoted to finding the extremal directions of the wave vector of a phase holographic grating (hereafter — grating) in the crystallographic coordinate system, along which the amplitude of the refractive index modulation in the GaAs crystal reaches its maximum values. It was shown that, among the crystallographic directions ⟨100⟩, ⟨110⟩, ⟨111⟩ and ⟨112⟩ the value of refractive index modulation in the GaAs crystal closest to the theoretical maximum can be achieved when the grating wave vector is oriented along the ⟨110⟩ direction. However, as shown in the earlier work [16], the GaAs crystal is characterized by the recording of mixed (phase-amplitude) gratings, where the presence of phase components is due to modulation of the dielectric permittivity of the recording medium, and the presence of amplitude components is due to modulation of nonlinear absorption upon the appearance of an electric field from spatially separated charges in the PRC. In [17] it was shown that, in addition to the phase component, accounting for the amplitude component of the mixed gratings formed in the GaAs crystal leads to better agreement between theoretical calculations of the orientation dependence of the reflection coefficient and experimental data. The issues of finding optimal conditions for FWM on phase gratings in the GaAs semiconductor were partially addressed in [18]. The work theoretically analyzed the dependence of the reflection coefficient on the crystal's orientation angle and thickness for the case where the pump and signal waves have *p*- or *s*-polarizations. It was shown that, in the absence of optical activity and at fixed polarization azimuths of the light waves, the optimal values of the orientation angle, for which the maximum reflection coefficient in FWM is achieved, remain constant if the crystal thickness does not exceed 8 mm. The results obtained in [18] are valid only in this specific case, since the analysis considered a GaAs crystal with a fixed cut plane and did not address the question of finding optimal values of the light wave polarization azimuths at which the reversed wave has maximum intensity.

In solving the problem of determining the most advantageous parameters of a holographic wavefront reversal setup in a PRC, at which the diffraction efficiency on dynamic gratings will be maximal, the optimal spatial orientation of the crystal must first be found. In the case of an unsuccessful choice of the crystal's spatial orientation, the amplitude changes in the refractive index and absorption coefficient of the mixed grating will take values close to zero, and the diffraction efficiency will be minimal regardless of the values of the other holographic setup parameters (e.g., crystal thickness and orientation angle, polarization azimuths and intensity ratio of the light waves, Bragg angles, etc.), as follows, e.g., from [19,20]. Upon selecting the optimal spatial orientation of the crystal, the diffraction efficiency on dynamic gratings can then be controlled by varying the holographic setup parameters, changing it from zero to the maximum possible. Since, in PRCs of symmetry class $\bar{4}3m$ the diffraction conditions are practically independent of crystal thickness due to the absence of optical activity, the length of optical interaction between the light waves can be disregarded when finding optimal FWM conditions for this class of nonlinear media. Further on, among the main parameters of the holographic setup, we will limit consideration to the influence of the crystal's orientation angle and the wave polarization azimuths on the reflection coefficient in FWM, as the diffraction efficiency on gratings in cubic PRCs is highly sensitive to their values [21,22].

The problem of finding the optimal spatial orientations of the photorefractive semiconductor GaAs relative to the plane of incidence, for which the highest diffraction efficiency in FWM is achieved, as well as determining the corresponding reflection coefficient values for such orientations, to the best of our knowledge, has not been addressed to date. In most studies, specific holographic configurations are examined, or the phase-amplitude structure of the gratings formed in such a crystal is not taken into account. Solving this problem would be highly useful for improving the efficiency of using GaAs semiconductors in optical applications through optimal tuning of the holographic setup.

The aim of this study is to determine the maximum values of the reflection coefficient in contradirectional degenerate frequency FWM on mixed gratings in the photorefractive semiconductor GaAs and to find the corresponding spatial orientations of the crystal relative to the plane of incidence of the holographic setup. The theoretical model will account for the combined action of the linear electro-optical, photoelastic, and inverse piezoelectric effects, as well as the natural absorption of the crystal and changes in the intensity of light waves due to their self-diffraction on the recorded gratings. The work will also include a comparative analysis between the reflection coefficient values optimized over the crystal's orientation angle and the azimuths of linear polarization of the light waves, calculated for the crystallographic directions ⟨100⟩, ⟨110⟩, ⟨111⟩ and ⟨112⟩.

Scheme of Four-Wave Mixing and Solution Method

Consider the geometric scheme of degenerate contradirectional FWM in the photorefractive semiconductor GaAs shown in Fig. 1, *a*. Linearly polarized pump waves *1, 2* and signal wave *3* induce the initial recording in the crystal of one transmission grating and two reflection gratings. As a result of scattering of the light waves on the primary gratings, the reversed wave *4* is formed, which is phase-conjugated with respect to the signal wave *3*. Pairwise interference of the reversed wave *4* with the pump waves *1,2* and signal wave *3* leads to the additional recording of secondary transmission and two reflection gratings. Thus, in contradirectional FWM, holographic recording in the PRC occurs in two stages, as a result of which up to six gratings can be formed [10,14]. To simplify the further analysis of the reversed wavefront formation patterns, we

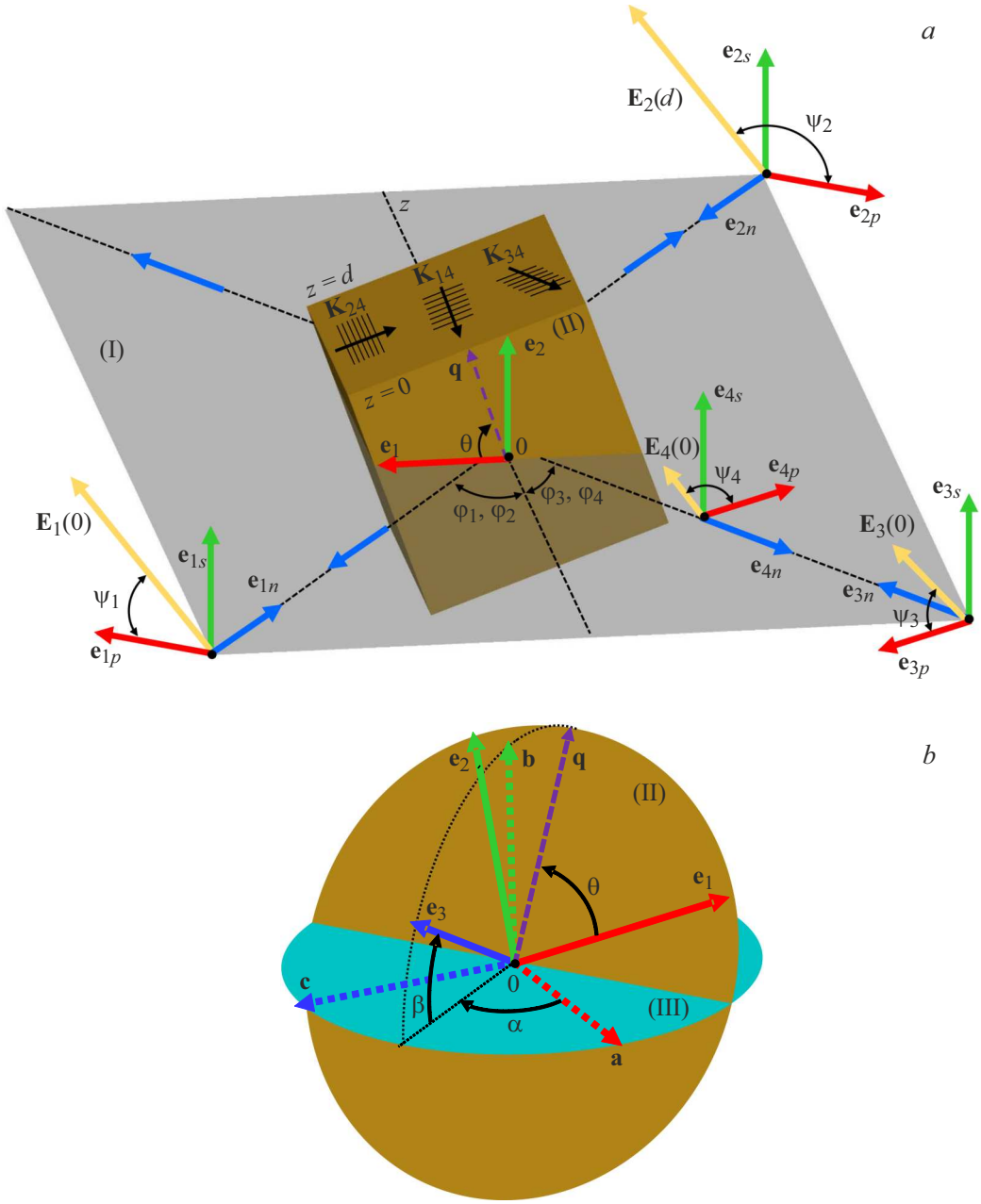

Figure 1. Geometric scheme of contradirectional four-wave mixing in a photorefractive crystal (a); definition of the mutual orientation of the crystallographic and laboratory coordinate systems via the angles α, β and θ (b).

will limit consideration to the diffraction contributions from only three secondary gratings. The secondary transmission grating *24*, whose wave vector $\mathbf{K}_{24}$ corresponds to Fig. 1, *a*, is formed as a result of interference between the reversed wave *4* and the pump wave *2*. The secondary reflection gratings *14* and *34*, arising from pairwise interference of the reversed wave *4* with the pump wave *1* and signal wave *3*, correspond to wave vectors $\mathbf{K}_{14}$ and $\mathbf{K}_{34}$. The parallel solid lines crossing the vectors $\mathbf{K}_{14}$, $\mathbf{K}_{24}$ and $\mathbf{K}_{34}$ conventionally depict the periodically arranged scattering planes of the corresponding gratings. The intensity of the reversed wavefront is the result of energy exchange between the light waves and is determined by the coherent summation of the diffraction contributions from the secondary gratings.

In Fig. 1, *a*, the orthonormal bases ($\mathbf{e}_{jp}$, $\mathbf{e}_{js}$, $\mathbf{e}_{jn}$), where $j = 1, 2, 3, 4$ are used to define the coordinate systems in which the propagation directions and polarization states of the light waves are specified. Vectors $\mathbf{e}_{jp}$ and $\mathbf{e}_{jn}$ lie in the plane of incidence (I), while vectors $\mathbf{e}_{js}$ are perpendicular to it. Vector $\mathbf{e}_{jn}$ coincides in direction with the wave normal j of the light wave. We assume that the light waves are linearly polarized, with corresponding vector amplitudes $\mathbf{E}_j$. The polarization azimuths ψ_j are used to specify the directions of the vectors $\mathbf{E}_j$ and are measured

from the vectors $\mathbf{e}_{jp}$ counterclockwise when looking against the corresponding wave normals of the light waves. The orthonormal basis ($\mathbf{e}_1$, $\mathbf{e}_2$, $\mathbf{e}_3$) is rigidly tied to the surface of the holographic table parallel to the plane of incidence (I) and is used to define the laboratory coordinate system. Note that vectors $\mathbf{e}_1$ and $\mathbf{e}_2$ lie in the crystal cut plane (II), while vector $\mathbf{e}_3$ is perpendicular to this plane. The unit vector $\mathbf{q}$ has a fixed direction in the crystallographic coordinate system and is fixed in the crystal cut plane (II) at the orientation angle θ to the vector $\mathbf{e}_1$. The thickness d is the length of optical interaction between the light waves and is measured along the axis $0z$ which coincides in direction with the vector $\mathbf{e}_3$. The Bragg angles φ_j are measured in the plane of incidence (I) between the axis $0z$ and the corresponding vectors $\mathbf{e}_{jn}$.

The method for specifying the spatial orientation of the semiconductor crystal grating relative to the laboratory coordinate system is illustrated in Fig. 1, *b*. The unit vectors of the orthonormal basis ($\mathbf{a}$, $\mathbf{b}$, $\mathbf{c}$) are parallel to the axes of the crystallographic coordinate system: $\mathbf{a} \parallel [100]$, $\mathbf{b} \parallel [010]$ and $\mathbf{c} \parallel [001]$. Plane (II) in Fig. 1, *b* coincides with the crystal cut plane (II) in Fig. 1, *a*. Plane (III) passes through the origin and contains the vectors $\mathbf{a}$ and $\mathbf{c}$. Vector $\mathbf{q}$ lies at the intersection of plane (II) with the plane containing the vectors $\mathbf{e}_3$ and $\mathbf{b}$. To find the spatial orientation of the crystal, it is necessary to specify the directions of the unit vectors ($\mathbf{a}$, $\mathbf{b}$, $\mathbf{c}$) in the laboratory coordinate system using the angles α, β and θ. The angles α and β fix the direction of the vector $\mathbf{e}_3$ in the crystallographic coordinate system. Since the vector $\mathbf{e}_3$ is perpendicular to the surface (II), specifying the angles α and β also determines the crystal cut plane. The orientation angle θ fixes the angle of crystal rotation relative to the vector $\mathbf{e}_3$ (axis $0z$). For example, for angles $\alpha = 90^\circ$ and $\beta = 135^\circ$ the crystal cut plane (II) becomes parallel to (110). In this case, for $\theta = 0^\circ$ the vector $\mathbf{q}$ in plane (II) is directed opposite to the vector $\mathbf{e}_2$ and with increasing orientation angle, it rotates counterclockwise when looking against the vector $\mathbf{e}_3$.

To find the polarization components $E_{4p}(0) = E_4(0)\cos\psi_4$ and $E_{4s}(0) = E_4(0)\sin\psi_4$ of the vector amplitude $\mathbf{E}_4(0)$ of the reversed wave 4, the coupled-wave equations given in [23] are used. Since the problem is considered taking into account the mutual influence of the mixed gratings recorded in the crystal and the recording light waves due to the self-diffraction effect, in the calculations, the components $E_{4p}(0)$ and $E_{4s}(0)$ are found as a result of the numerical solution of the coupled-wave equations using the well-known shooting method [24]. In this case, the coupled-wave equations represent a two-point boundary value problem with initial conditions: $E_{1p}(0) = E_1\cos\psi_1$, $E_{1s}(0) = E_1\sin\psi_1$, $E_{2p}(d) = E_2\cos\psi_2$, $E_{2s}(d) = E_2\sin\psi_2$, $E_{3p}(0) = E_3\cos\psi_3$, $E_{3s}(0) = E_3\sin\psi_3$, $E_{4p}(d) = E_4\cos\psi_4$, $E_{4s}(d) = E_4\sin\psi_4$. The analytical expressions used to find the changes in the components of the inverse dielectric permittivity tensor of a cubic PRC arising during the recording of a phase grating are given in [25]. The diffraction efficiency in wavefront reversal is determined via the reflection coefficient R, which is equal to the ratio [14]: $I_4(0)/I_3(0)$, where $I_3(0)$ and $I_4(0)$ — intensities of the signal and reversed waves at $z = 0$.

To find the spatial orientations of the crystal at which the highest wavefront reversal efficiency is achieved, it is necessary to investigate the dependence of the reflection coefficient R^{opt} optimized over the polarization azimuths ψ_1, ψ_2, ψ_3 and the orientation angle θ on the direction of the vector $\mathbf{e}_3$ in the crystallographic coordinate system. For a fixed orientation of the vector $\mathbf{e}_3$ (α, $\beta = \text{const}$) the optimized reflection coefficient R^{opt} is found by determining the maximum value from an array of reflection coefficient values obtained by enumerating physically distinct values of the orientation angle and polarization azimuths. By repeating this procedure for various values of the angles α and β an optimized reflection coefficient R^{opt} can be assigned to each direction of the vector $\mathbf{e}_3$ in the crystallographic coordinate system. The directions of the vector $\mathbf{e}_3$, for which R^{opt} takes the maximum value ($R^{\text{opt}} = R^{\max}$) will correspond to the optimal spatial orientations of the crystal in FWM. To visualize the obtained results in the crystallographic coordinate system, a surface $R^{\text{opt}}(\mathbf{e}_3)$ [26] is constructed, the position vector of which is proportional to the values of R^{opt} in the given direction of the vector $\mathbf{e}_3$. By definition, the reflection coefficient can take only positive values, and therefore all points of the surface $R^{\text{opt}}(\mathbf{e}_3)$ are colored uniformly.

In the numerical solution of the coupled-wave equations, the following material parameters of the GaAs crystal at the wavelength $\lambda = 1064 \cdot 10^{-9}$ m were used: refractive index of the unperturbed crystal $n_0 = 3.48$ [16]; electro-optical coefficient $r_{41} = -1.43 \cdot 10^{-12}$ m/V [16]; elastic constants $c_1 = 11.88 \cdot 10^{10}$ N/m^2, $c_2 = 5.38 \cdot 10^{10}$ N/m^2, $c_3 = 5.94 \cdot 10^{10}$ N/m^2 [16]; photoelastic coefficients $p_1 = -0.165$, $p_2 = p_3 = -0.14$, $p_4 = -0.072$ [27]; piezoelectric coefficient $e_{14} = 0.154$ C/m^2 [16]. Here, the following notations are adopted for the nonzero components of the tensors of the linear electro-optical ($\hat{r}$), photoelastic ($\hat{p}$) and inverse piezoelectric ($\hat{e}$) effects, as well as the elasticity tensor components ($\hat{c}^E$): $r^S_{123}=r^S_{132}=r^S_{213}=r^S_{231}=r^S_{312}=r^S_{321}\equiv r_{41}$, $e_{123} = e_{132} = e_{213} = e_{231} = e_{312} = e_{321} \equiv e_{14}$, $c^E_{11} = c^E_{22} = c^E_{33} \equiv c_1$, $c^E_{12}=c^E_{13}=c^E_{23}=c^E_{21}=c^E_{31}=c^E_{32}\equiv c_2$, $c^E_{44} = c^E_{55} = c^E_{66} \equiv c_3$, $p^E_{11} = p^E_{22} = p^E_{33} \equiv p_1$, $p^E_{12} = p^E_{23} = p^E_{31} \equiv p_2$, $p^E_{13} = p^E_{21} = p^E_{32} \equiv p_3$, $p^E_{44} = p^E_{55} = p^E_{66} \equiv p_4$. Note that, for PRCs of class $\bar{4}3m$ in accordance with the symmetry rules, the components p_2 and p_3 are equal to each other. The linear absorption coefficient of the crystal is taken to be $\alpha = 30\,\text{m}^{-1}$. In the calculations, the phase components of the mixed gratings are assumed to be spatially shifted by a quarter period relative to the recording interference patterns, while the amplitude components are unshifted. In selecting the polarization azimuths ψ_j we follow the rule that the electric field vectors $\mathbf{E}_j$ remain parallel to each other during wave propagation in the crystal, which holds under the condition: $\psi_1 = \psi_2 = 180^\circ - \psi_3 = \psi$.

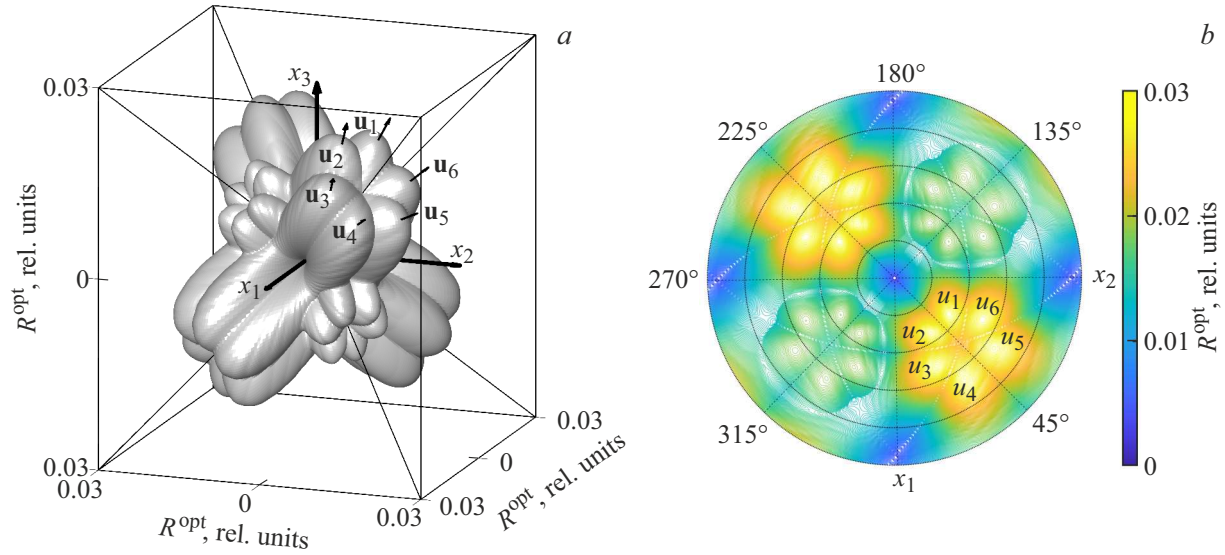

Figure 2. Indicatrix surface of the dependence of optimized reflection coefficient values on the spatial orientation of the crystal (a); indicatrix surface in stereographic projection onto the x_1x_2 plane (b).

The amplitudes of the electric field of spatially separated charges during the formation of mixed gratings in the PRC are taken to be 2 kV/cm. The coefficients used in [23] to specify the coupling between waves during their diffraction on the amplitude components of the mixed gratings are taken to be $20\,\mathrm{m}^{-1}$. The Bragg angle in the crystal in solving the coupled-wave equations is taken to be 5°.

Due to the high holographic sensitivity of the GaAs crystal, in most studies, light beams with intensity densities from several tens to hundreds of $\mathrm{mW/cm}^2$ were used for grating recording (see, e.g., [14,16,21]). The data presented in this work were obtained for the same range of intensity densities, with the pump wave intensities at the crystal input taken to be equal to each other in the calculations, and their ratio to the initial signal wave intensity being 20 : 1. The optimization results given below are independent of changes in light wave intensities only if the ratios between them are preserved. If the initial intensity values are chosen such that the assumed ratios between them in the calculations are violated, the results of the work should be recalculated using the method described above.

Results and Discussion

Fig. 2, a shows the surface $R^{\mathrm{opt}}(\mathbf{e}_3)$, illustrating the dependence of the optimized reflection coefficient values R^{opt} on the spatial orientation of the GaAs crystal, specified via the direction of the vector $\mathbf{e}_3$. The crystallographic coordinate system is denoted by vectors: $x_1 \parallel [100]$, $x_2 \parallel [010]$, $x_3 \parallel [001]$. Thin solid lines parallel to the $\langle 100 \rangle$ axes are an additional construction to display the scale with divisions of the measured physical quantity. Diagonal thin solid lines parallel to the $\langle 111 \rangle$ axes are used for convenience in examining the external symmetry of the constructed surface.

The surface $R^{\mathrm{opt}}(\mathbf{e}_3)$ is a symmetric figure that can be superimposed on itself by symmetry transformations. The external symmetry of the surface $R^{\mathrm{opt}}(\mathbf{e}_3)$ in accordance with Neumann's principle [26] includes the full set of symmetry elements of the crystal polyhedron of the planar class of the cubic syngony. Along the $\langle 100 \rangle$ directions are the fourth-order symmetry inversion axes, since the figure superimposes on itself under symmetric transformation involving rotation by 90° about the axes and reflection through the origin. The figure superimposes upon rotation by 120° about the third-order symmetry rotation axes directed along $\langle 111 \rangle$. The external symmetry of the figure also corresponds to six symmetry planes located parallel to $\{110\}$. The described symmetry elements fully match the point symmetry group of the GaAs crystal polyhedron.

As follows from Fig. 2, a, the extremal directions of the surface, for which the condition $R^{\mathrm{opt}} = R^{\max}$ holds, are symmetrically equivalent and differ from the standard crystallographic directions $\langle 100 \rangle$, $\langle 110 \rangle$, $\langle 111 \rangle$ and $\langle 112 \rangle$, considered in the literature (see, e.g., [16,19–21,28]). The maximum values of the optimized reflection coefficient are achieved along a set of symmetrically equivalent directions $\langle 234 \rangle$. As an example, in Fig. 2, a, the beam of vectors $\mathbf{u}_1 - \mathbf{u}_6$ denotes the extremal directions ($\mathbf{u}_1 \parallel [234]$, $\mathbf{u}_2 \parallel [324]$, $\mathbf{u}_3 \parallel [423]$, $\mathbf{u}_4 \parallel [432]$, $\mathbf{u}_5 \parallel [342]$ and $\mathbf{u}_6 \parallel [243]$), symmetrically arranged relative to the axis [111], along which the optimized reflection coefficient reaches its absolute maximum $R^{\max} = 2.8 \cdot 10^{-2}$. The directions $\langle 234 \rangle$ are polar [26], since the position vectors laid off along such directions in opposite senses to the points of the surface $R^{\mathrm{opt}}(\mathbf{e}_3)$ have different magnitudes and do not superimpose on each other by symmetry transformations. For example, along the direction [234], the maximum value of the optimized reflection coefficient $R^{\max} = 2.8 \cdot 10^{-2}$

is achieved, while in the opposite direction $[\bar{2}\,\bar{3}\,\bar{4}]$ the parameter R^{opt} equals $2 \cdot 10^{-2}$.

For a more precise depiction of the symmetry of the figure under consideration, Fig. 2, *b* shows the stereographic projection of the surface $R^{\text{opt}}(\mathbf{e}_3)$ onto the plane passing through the origin of the crystallographic coordinate system and parallel to (001). The stereographic projections of the vectors $\mathbf{u}_1 - \mathbf{u}_6$ and the direction [111] are shown in the plot. From Fig. 2, *b*, it is evident that, for the surface under study in the vicinity of the third-order rotation axes, there is a set of six symmetrically arranged maxima of the function $R^{\text{opt}}(\mathbf{e}_3)$ achieved along the extremal directions ⟨234⟩. At the same time, as follows from Fig. 2, if six absolute maxima ⟨111⟩ are symmetrically located on one side of the ($R^{\max} = 2.8 \cdot 10^{-2}$) parallel rotation axis, then six local maxima ($R^{\text{opt}} = 2 \cdot 10^{-2}$) are on the opposite side. Since the difference in R^{opt} values between the absolute and local maxima of the surface $R^{\text{opt}}(\mathbf{e}_3)$ reaches nearly 25%, when setting up the holographic setup, the asymmetry of energy exchange between light waves upon changing the spatial orientation of the crystal sample by 180° should be taken into account.

The data presented in Fig. 2 allow determination of the extremal directions and assessment of the external symmetry of the surface $R^{\text{opt}}(\mathbf{e}_3)$. However, to compare the optimized reflection coefficient values achieved when using typical spatial orientations of the GaAs crystal for experimental studies ($\mathbf{e}_3 \parallel$ ⟨100⟩, ⟨110⟩, ⟨111⟩, ⟨112⟩) the corresponding sections of the figure must be analyzed. In Fig. 3, *a*–6, *a* the mutual orientations of the surface and the section planes passing through the origin are shown, depicted as gray polygons. The shape of the polygons corresponds to the geometric locus of points of the section planes that lie within the volume of the cube bounded by solid lines parallel to the ⟨100⟩ axes. In Fig. 3, *b*–6, *b* the traces of the surface intersection with the section planes are shown as black solid lines. For convenience in examining the figures, certain crystallographic directions in the section plane are additionally shown as vectors. In addition, to facilitate finding the extremal directions in the section plane, dashed circles are constructed, the radii of which correspond to the points where the surface intersects the maximum value of R^{opt}. The position vector drawn from the origin to the point of tangency of the surface section with the dashed circle will be one of the extremal directions of the section.

Fig. 3 shows the trace of the intersection of the surface $R^{\text{opt}}(\mathbf{e}_3)$ with the (100)-parallel section plane. Consideration of the section plane with this spatial orientation is motivated by the need for comparative analysis of optimized reflection coefficients in holographic configurations where the vector $\mathbf{e}_3$ is parallel to the ⟨100⟩ and ⟨110⟩ directions. As seen from Fig. 3, *b*, the section of the surface $R^{\text{opt}}(\mathbf{e}_3)$ is a plane figure that superimposes on itself upon rotation by 90° which, in accordance with Neumann's principle, is explained by the perpendicularity of the section plane to the fourth-order symmetry rotation axis. The crystallographic directions ⟨100⟩ and ⟨110⟩ are centro-symmetric, as identical values

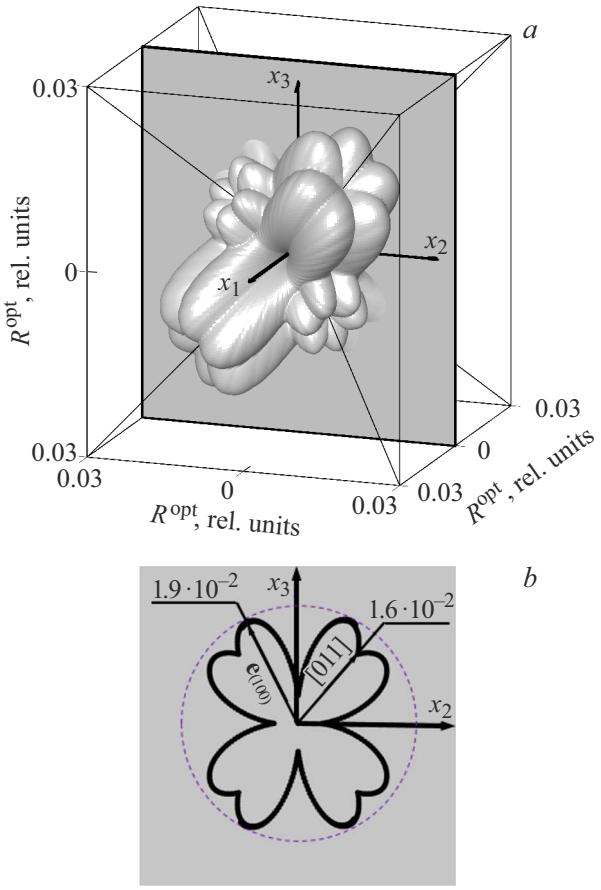

Figure 3. Mutual arrangement of the indicatrix surface and the (100)-parallel section plane (*a*); trace of the indicatrix surface in the section plane (*b*).

of R^{opt} are achieved along lines parallel to these directions. In the case where the crystal cut plane (II) is parallel to one of the planes of the {100} family ($\mathbf{e}_3 \parallel$ ⟨100⟩), the reflection coefficient under optimal conditions reaches $R^{\text{opt}} = 5 \cdot 10^{-3}$. A threefold higher reflection coefficient value can be achieved when plane (II) is parallel to {110}, since when the vector $\mathbf{e}_3$ is oriented along the ⟨110⟩ directions, the parameter R^{opt} is approximately$1.6 \cdot 10^{-2}$. However, the ⟨100⟩ and ⟨110⟩ directions are not extremal — in the (100)-parallel section plane, there exist directions along which the optimized reflection coefficient reaches its local maximum $R^{\text{opt}} = 1.9 \cdot 10^{-2}$. To find the extremal directions, position vectors should be drawn from the origin to the four symmetrically located points of tangency of the dashed circle with the surface section $R^{\text{opt}}(\mathbf{e}_3)$. For greater clarity, in Fig. 3, *b*, one such extremal direction is marked by the vector $\mathbf{e}_{(100)}$, which is oriented at an angle 30° to the x_3 axis.

To compare the R^{opt} values that can be achieved along the ⟨110⟩ and ⟨111⟩ directions, consider Figs. 4 and 5, which illustrate the sections of the surface $R^{\text{opt}}(\mathbf{e}_3)$ by planes parallel to (110) and (112). As follows from the presented data, if the front face of the crystal (II)

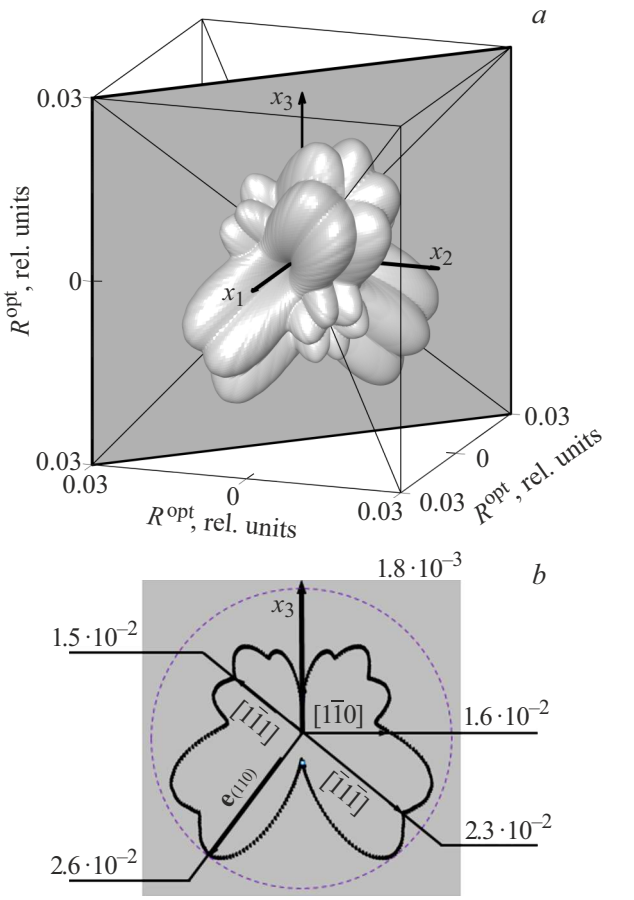

Figure 4. Mutual arrangement of the indicatrix surface and the (110)-parallel section plane (a); trace of the indicatrix surface in the section plane (b).

is parallel to one of the set of symmetrically equivalent {111} planes, corresponding to the case $\mathbf{e}_3 \parallel \langle 111 \rangle$, then under optimal conditions, the reflection coefficient can reach $2.3 \cdot 10^{-2}$. This is approximately 4.6 and 1.35 times higher than in the previously considered cases where $\mathbf{e}_3 \parallel \langle 100 \rangle$ and $\mathbf{e}_3 \parallel \langle 110 \rangle$ respectively. It should be noted that, unlike $\langle 100 \rangle$ and $\langle 110 \rangle$ the $\langle 111 \rangle$ directions are polar, and the position vectors oriented along the third-order symmetry rotation axes in opposite directions, whose magnitude equals R^{opt} do not superimpose by symmetry transformations. For example, in Fig. 4, b, the value of R^{opt} in the $[\bar{1}1\bar{1}]$ direction is $2.3 \cdot 10^{-2}$ while along $[1\bar{1}1]$ it is $1.5 \cdot 10^{-2}$. Due to the symmetry of the surface $R^{opt}(\mathbf{e}_3)$ an analogous difference in optimized reflection coefficient values is achieved for the $[\bar{1}\,\bar{1}\,1]$ and $[11\bar{1}]$ directions (Fig. 5, b). The $\langle 111 \rangle$ directions are not extremal in Figs. 4, b and 5, b — in the section planes, there exist directions along which the parameter R^{opt} reaches higher values than at $\mathbf{e}_3 \parallel \langle 111 \rangle$. In the (110)-parallel section plane, the local maximum of the parameter R^{opt} is $2.6 \cdot 10^{-2}$ and is achieved along two symmetrically located extremal directions that form angles x_3 with the 144° axis. One such direction is denoted by the vector $\mathbf{e}_{(110)}$ in Fig. 4, b. In the (112)-parallel section plane, two extremal directions can also be noted, one of which coincides with the vector $\mathbf{e}_{(112)}$ and forms an angle 16° with the vertical x_3 axis. In this case, when the vector $\mathbf{e}_3$ is oriented along the extremal direction, R^{opt} is $2.5 \cdot 10^{-2}$.

Fig. 6 shows the section of the surface $R^{opt}(\mathbf{e}_3)$ by the (111)-parallel plane. As seen from Fig. 6, b, the trace of the figure's intersection with the section plane is a plane symmetric figure that can be superimposed on itself upon rotation by 120°, which is consistent with Neumann's principle, as the section plane is perpendicular to the third-order symmetry rotation axis. From Fig. 6, b, it is evident that the $\langle 112 \rangle$ directions are also polar, and the lines passing through them intersect the surface $R^{opt}(\mathbf{e}_3)$ at $R^{opt} = 2.5 \cdot 10^{-2}$ and $R^{opt} = 1.7 \cdot 10^{-2}$. The optimized reflection coefficient achieved along the $\langle 112 \rangle$ direction is 90% of the maximum possible value R^{max} and exceeds the R^{opt} value corresponding to the $\langle 111 \rangle$ directions by approximately 10%. The diffraction efficiency on mixed gratings when the vector $\mathbf{e}_3$ is oriented along the $\langle 110 \rangle$ directions is substantially lower than along the $\langle 112 \rangle$ directions, as follows from the 40% difference between the R^{opt} values achieved along the $[\bar{1}1\bar{2}]$ and $[\bar{1}10]$

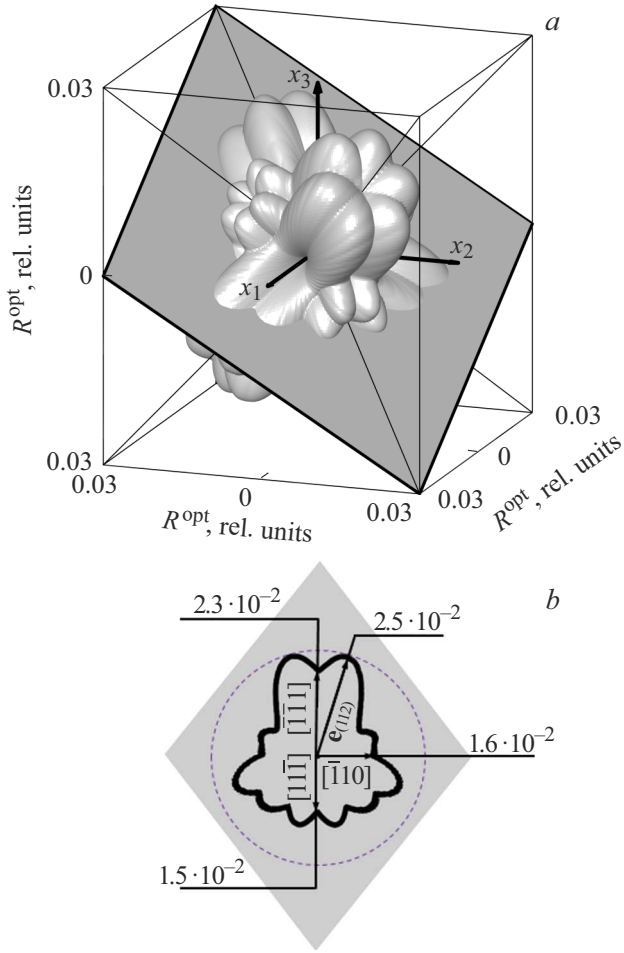

Figure 5. Mutual arrangement of the indicatrix surface and the (112)-parallel section plane (a); trace of the indicatrix surface in the section plane (b).

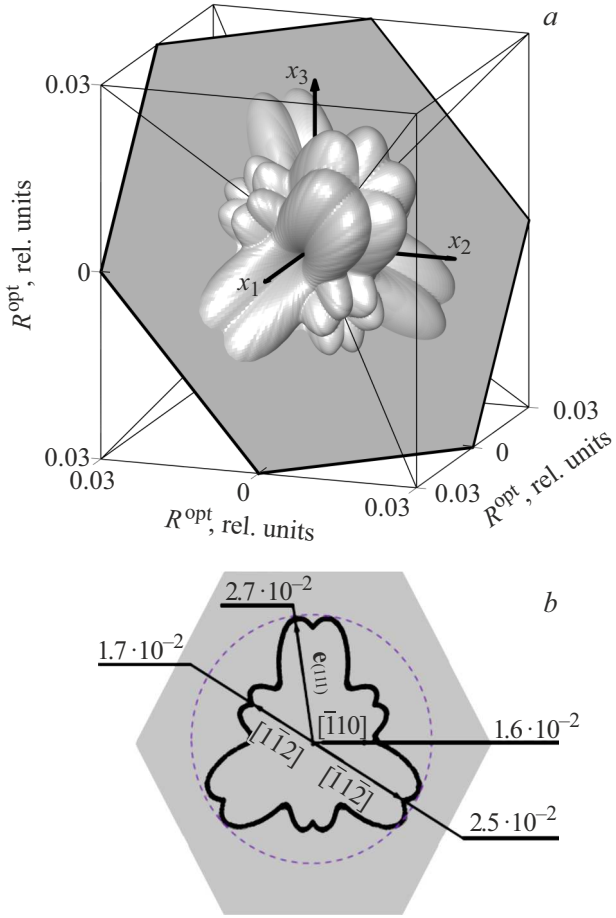

Figure 6. Mutual arrangement of the indicatrix surface and the (111)-parallel section plane (*a*); trace of the indicatrix surface in the section plane (*b*).

directions in Fig. 6, *b*. In the section plane, the maximum value of the parameter $R^{opt} = 2.7 \cdot 10^{-2}$ is achieved along six symmetrically located extremal directions that do not coincide with $\langle 110 \rangle$ and $\langle 112 \rangle$. In Fig. 6, *b*, one such direction is denoted by the vector $\mathbf{e}_{(111)}$, which forms an angle 98° with $[\bar{1}10]$.

Conclusion

The optimal spatial orientations of the photorefractive crystal with GaAs material parameters, at which the highest wavefront reversal efficiency on secondary mixed (phase-amplitude) gratings is achieved, have been determined theoretically. It has been shown that the reflection coefficient R^{opt} optimized over the crystal's orientation angle and the azimuths of linear polarization of the light waves, reaches its maximum value ($R^{max} = 2.8 \cdot 10^{-2}$) in cases where the vector $\mathbf{e}_3$ normal to the cut plane of the crystal sample is directed along one of the $\langle 234 \rangle$ directions. Among the crystal samples commonly used in holographic experiments, for which the vector $\mathbf{e}_3$ is oriented along one of the directions $\langle 100 \rangle$, $\langle 110 \rangle$, $\langle 111 \rangle$ or $\langle 112 \rangle$, the most advantageous is the GaAs crystal for which the vector $\mathbf{e}_3$ is parallel to $\langle 112 \rangle$. In this case, the optimized reflection coefficient reaches 90% of the maximum possible value. When the vector $\mathbf{e}_3$ is oriented along the $\langle 111 \rangle$ directions, wavefront reversal efficiency close to the highest can also be achieved, since the optimized reflection coefficient reaches 80% of the maximum value. Choosing the spatial orientation of the GaAs crystal such that the vector $\mathbf{e}_3$ is parallel to the $\langle 110 \rangle$ directions is less advantageous in terms of achieving higher intensities of the reversed wave, as in this case the optimized reflection coefficient is about 50% of the maximum. The lowest wavefront reversal efficiency among typical spatial orientations of the GaAs crystal is achieved for the $\langle 100 \rangle$ directions, as the reflection coefficient in FWM does not exceed 20% of the maximum possible value.

The obtained results can be applied to improve the efficiency of using photorefractive GaAs semiconductors in optical applications by selecting the optimal spatial orientation of the crystal when setting up the holographic setup. At the same time, when considering the presented data, it should be borne in mind that if the crystal material parameters or holographic setup parameters deviate from those used in the work, the extremal directions of the surface $R^{opt}(\mathbf{e}_3)$, along which maximum reflection coefficient values are achieved, may change. Therefore, further development of research in this direction appears to involve performing similar studies for semiconductors with InP and CdTe parameters, as well as crystals with sillenite structure $Bi_{12}TiO_{20}$, $Bi_{12}SiO_{20}$, $Bi_{12}GeO_{20}$.

Funding

The work was carried out with financial support from the Ministry of Education of the Republic of Belarus (contract dated March 22, 2021 No 1410/2021) under the State Program of Scientific Research „Photonics and Electronics for Innovations“ for 2021–2025.

Conflict of interest

The author declares that he has no conflict of interest.

References

[1] V.M. Petrov, A.V. Shamray. Interferenciya i difrakciya dlya informacionnoj fotoniki (Lan, SPb., 2019), 460 p. (in Russian)
[2] A. Katti, R.A. Yadav. Optical spatial solitons in photorefractive materials (Springer Nature, Singapore, 2021), 169 p. DOI: 10.1007/978-981-16-2550-3
[3] E.A. Vlieg, L. Talandier, R. Dangel, F. Horst, B.J. Offrein. Appl. Sci., **12**, 4226 (2022). DOI: 10.3390/app12094226
[4] A. Bile, H. Tari, E. Fazio. Appl. Sci., **12**, 5585 (2022). DOI: 10.3390/app12115585
[5] A. Bile, H. Tari, R. Pepino, A. Nabizada, E. Fazio. Biomimetics, **9**, 231 (2024). DOI: 10.3390/biomimetics9040231

[6] S.M. Shandarov, V.M. Shandarov, A.E. Mandel, N.I. Burimov. *Fotoreaktivnye effekty v elektroopticheskikh kristallakh* (TUSUR, Tomsk, 2012), 242 p. (in Russian).
[7] J. Frejlich. *Photorefractive materials for dynamic optical recording: fundamentals, characterization, and technology* (John Wiley & Sons Inc., Hoboken, 2020), 310 p.
[8] B.I. Stepanov, E.V. Ivakin, A.S. Rubanov. Dokl. Akad. Nauk SSSR, **196** (3), 567 (1971) (in Russian).
[9] I.G. Dadenkov, A.L. Tolstik, Yu.I. Miksyuk, K.A. Saechnikov. Opt. Spectrosc., **128** (9), 1401 (2020). DOI: 10.1134/S0030400X20090052
[10] S.G. Odulov, M.S. Soskin, A.I. Khizhnyak, *Lazery na dinamicheskikh reshetkakh: opticheskie generatory na chetyrekhvolnovom smeshenii* (Nauka, M., 1990), 272 p. (in Russian).
[11] G.J. de Valcárcel, F. Silva, A. Esteban-Martín, E. Roldán. J. Opt., **25** (7), 075502 (2023). DOI: 10.1088/2040-8986/accfab
[12] H. Zhou, Y. Duan, H. Song, X. Su, Z. Zhao, K. Zou, H. Song, R. Zhang, R.W. Boyd, M. Tur, A.E. Willner. Opt. Lett., **48** (8), 2194 (2023). DOI: 10.1364/OL.487133
[13] K. Shcherbin, P. Mathey, A.N. Shumelyuk, D.R. Evans. JOSA B, **41** (11), 2502 (2024). DOI: 10.1364/JOSAB.534061
[14] M.P. Petrov, S.I. Stepanov, A.V. Knomenko. *Photoreaktivnye kristally v kogerentnoi optike* (Nauka, SPb., 1992) (in Russian).
[15] V.N. Navnyko. FTT, **66** (2), 198 (2024) (in Russian). DOI: 10.61011/FTT.2024.02.57243.268
[16] K. Shcherbin, S. Odoulov, R. Litvinov, E. Shandarov, S. Shandarov. J. Opt. Soc. Am. B, **13** (10), 2268 (1996). DOI: 10.1364/JOSAB.13.002268
[17] V.N. Naunyka. Opt. Spectrosc., **130** (3), 324 (2022). DOI: 10.21883/EOS.2022.03.53557.2936-21.
[18] V.N. Naunyka. Bulletin of the Russian Academy of Sciences: Physics, **86** (Suppl. 1), S145 (2022). DOI: 10.3103/S1062873822700575
[19] H.J. Eichler, Y. Ding, B. Smandek. Phys. Rev. A, **52** (3), 2411 (1995). DOI: 10.1103/physreva.52.2411
[20] N.C. Deliolanis, I.M. Kourmoulis, A.G. Apostolidis, E.D. Vanidhis, D.G. Papazoglou. Phys. Rev. E, **68**, 056602 (2003). DOI: 10.1103/PhysRevE.68.056602
[21] Y. Ding, H.J. Eichler. Opt. Commun., **110**, 456 (1994). DOI: 10.1016/0030-4018(94)90449-9
[22] A.V. Gusel'nikova, S.M. Shandarov, A.M. Plesovskikh, R.V. Romashko, Yu.N. Kulchin. J. Opt. Technol., **73** (11), 760 (2006). DOI: 10.1364/JOT.73.000760.
[23] V.N. Navnyko. ZhTF, **94** (11), 1854 (2024) (in Russian). DOI: 10.61011/JTF.2024.11.59103.212-24
[24] Y.H. Ja. Opt. and Quant. Electron., **15**, 539 (1983). DOI: 10.1007/bf00620022
[25] S.M. Shandarov, V.V. Shepelevich, N.D. Khatkov. Opt. i spektr., **70** (5), 1068 (1991). (in Russian).
[26] M.P. Shaskol'skaya. *Kristallografiya* (Vysshaya shkola, M., 1984), 376 p. (in Russian)
[27] A. Dargys, J. Kundrotas. *Handbook on physical properties of Ge, Si, GaAs, InP* (Science and Encyclop. Publishers, Vilnius, 1994), 264 p.
[28] V.P. Kamenov, Y. Hu, E. Shamonina, K.H. Ringhofer, V.Ya. Gayvoronsky. Phys. Rev. E, **62** (2), 2863 (2000). DOI: 10.61011/JTF.2024.11.59103.212-24

Translated by J.Savelyeva